

A Comparative Analysis of Contact Models in Trajectory Optimization for Manipulation*

Aykut Onol, Philip Long, and Taskin Padir¹

Abstract—In this paper, we analyze the effects of the contact model on contact-implicit trajectory optimization for manipulation. We consider three different cases: (1) a contact model that is based on complementarity constraints, (2) a smooth contact model, and our proposed method (3) a variable smooth contact model. We compare these models in simulation in terms of quality of motions discovered, physical accuracy, and computation time. In each case, optimization is initialized by setting all decision variables to zero, namely, without a meaningful initial guess. For simulations, we consider a pushing manipulation task with varying complexity for a 7 degrees-of-freedom robot arm. Our results demonstrate that the optimization based on the proposed variable smooth contact model provides a good trade-off between the physical fidelity and the quality of motions discovered at the cost of increased computation time.

I. INTRODUCTION

Discovering contact-rich motions for manipulation and locomotion tasks without a predefined contact schedule is a captivating idea. Thus, contact-implicit trajectory optimization attracted many researchers from fields such as robotics, computer graphics, and bio-mechanics. Main idea of this approach is to define an optimization problem with costs and constraints describing a task of interest so that contact forces and a contact schedule are found as a result of trajectory optimization rather than using a predefined schedule.

In contact-implicit trajectory optimization, the selection of contact model is crucial since it provides optimization with a way to reason about contacts. The complementarity constraints have been extensively used for this purpose. A time-stepping scheme that use nonlinear complementarity constraints to model rigid-body dynamics with inelastic collisions and Coulomb friction was first proposed by Stewart & Trinkle [1]. Anitescu & Potra [2] show that such a problem can be formulated as solvable linear complementarity problems. In [3], Posa et al. propose a direct contact-implicit trajectory optimization method based on the time-stepping scheme in [1] to prevent “combinatorial explosion” of hybrid models. Indeed, the idea of transcribing a non-smooth trajectory optimization problem with impacts and discontinuities into a nonlinear optimization problem with complementarity constraints was first introduced by Yunt & Glocker [4]. However, in [4], the optimization of control inputs is decoupled from the optimization of states and contact

forces; whereas, in [3], they are all optimized simultaneously. Nonetheless, in both methods, contact dynamics is modeled as a complementarity problem. [5] uses complementarity constraints as well but within a hierarchical approach.

On the other hand, smooth contact models facilitate convergence of gradient-based solvers. For this reason, [6–9] use smoother fragments of complementarity constraints; whereas [10–12] directly define contact models as smooth functions of distance. In [13] and [14], contacts are modeled within the cost function by using auxiliary variables. In addition, there are other contact modeling approaches that fall outside of this classification such as the ones in [15] and [16].

Although contact-implicit trajectory optimization is, by definition, independent of task and can be generalized to both locomotion and manipulation tasks, a significant part of the related literature focuses on locomotion tasks (e.g., [5], [7–9], [12], [16]). Nonetheless, for instance, [3], [13], [14], [17] investigate manipulation tasks but their analysis is either limited to planar case or based on animated characters (i.e., physical realism is not as critical as in robotics).

Thus, in this study, we tackle with a manipulation problem and analyze the impact of contact model on the performance of contact-implicit trajectory optimization. We investigate a complementarity constraints-based contact model (CCCM), a smooth contact model (SCM), and a variable smooth contact model (VSCM) that we propose. For simulations, we consider the nonprehensile manipulation task of pushing a cubic object on a tabletop by a Sawyer robot which has a 7 degrees-of-freedom (DOF) arm. For modeling and simulations, we use the Multi-Joint dynamics with Contact (MuJoCo) physics engine [18] since it is shown to be favorable for robotic systems [19]. Optimization problems are solved through a sequential quadratic programming (SQP) solver called sparse nonlinear optimizer (SNOPT) [20]. Additionally, we use IFOPT [21] as an interface between MuJoCo and SNOPT.

The paper is organized as follows. In Section II, we describe the dynamical model of the system, the contact models, and the corresponding optimization problems. The results and their analysis are presented in Section III. Finally, concluding remarks and the future research directions are given in Section III.

II. METHODOLOGY

A. Dynamical Model

The dynamics of an n DOF robot that is in contact with environment can be obtained through Euler-Lagrange

*This research is supported by the Department of Energy under Award Number DE-EM0004482, by the National Aeronautics and Space Administration under Grant No. NNX16AC48A issued through the Science and Technology Mission Directorate and by the National Science Foundation under Award No. 1451427.

¹Robotics and Intelligent Vehicles Research Lab, Northeastern University, Boston, MA, USA {aonol, plong, tpadir}@ece.neu.edu

equations:

$$\mathbf{M}(\mathbf{q})\ddot{\mathbf{q}} + \mathbf{C}(\mathbf{q}, \dot{\mathbf{q}}) = \boldsymbol{\tau} + \mathbf{J}_c(\mathbf{q})^T \boldsymbol{\lambda}_c, \quad (1)$$

where $\mathbf{q}, \dot{\mathbf{q}}, \ddot{\mathbf{q}} \in \mathbb{R}^n$ are the joint positions, velocities, and accelerations, respectively; $\mathbf{M}(\mathbf{q}) \in \mathbb{R}^{n \times n}$ is the inertial matrix; $\mathbf{C}(\mathbf{q}, \dot{\mathbf{q}}) \in \mathbb{R}^n$ represents the Coriolis, centrifugal, and gravitational terms; $\boldsymbol{\tau}$ is the joint torques; $\mathbf{J}_c(\mathbf{q}) \in \mathbb{R}^{6n_c \times n}$ is the Jacobian matrix mapping the joint velocities to the Cartesian velocities at the contact points; and $\boldsymbol{\lambda}_c \in \mathbb{R}^{6n_c}$ is the generalized contact forces at the contact points for n_c potential contacts.

In this study, we use the MuJoCo physics engine [18] to model the dynamics and run forward simulations by using the fourth-order Runge-Kutta integrator with time steps of 5 ms and the Newton solver for the constraints. Moreover, we decouple the vector of joint torques as follows:

$$\boldsymbol{\tau} = \mathbf{u} + \hat{\mathbf{C}}(\mathbf{q}, \dot{\mathbf{q}}) - \mathbf{J}_c(\mathbf{q})^T \boldsymbol{\lambda}_c, \quad (2)$$

where $\hat{\mathbf{C}}(\mathbf{q}, \dot{\mathbf{q}})$ is an estimation of $\mathbf{C}(\mathbf{q}, \dot{\mathbf{q}})$, $\boldsymbol{\lambda}_c$ is calculated from the magnitude of normal contact force that is determined by either optimization or contact model, and $\mathbf{u} \in \mathbb{R}^n$ is the control input that is handled by the optimization. As a result, the robot can do gravity compensation even though the control input is zero. Furthermore, the third term eliminates the joint torques due to contacts and eases stabilization of the robot when there are contact forces. In our experiments, we observe that this decoupling of $\boldsymbol{\tau}$ improves the optimization results significantly.

B. Contact Model

In this study, we investigate the following three contact models. Contact forces on the tangential plane (i.e., frictional forces) are not considered in any of the models since we are not interested in generating such forces here. However, an elliptic approximation of the Coulomb friction cone is taken into account in the simulations owing to MuJoCo.

1) *Complementarity Constraints-based Contact Model:* Complementarity constraints that represent rigid-body contact are given by:

$$\phi(\mathbf{q}) \geq 0, \quad (3)$$

$$\gamma \geq 0, \quad (4)$$

$$\gamma^T \phi(\mathbf{q}) = 0, \quad (5)$$

where $\phi(\mathbf{q}) : \mathbb{R}^n \rightarrow \mathbb{R}^{n_c}$ is the signed distance function mapping the joint positions to the closest distance between bodies, i.e., (3) prevents interpenetration between bodies. $\gamma \in \mathbb{R}^{n_c}$ is the Lagrange multiplier that physically corresponds to the magnitude of the normal contact force, thus (4) ensures bodies can only push each other. Equation (5), which is evaluated element-wise due to computational reasons ([3], [22]), guarantees that either distance or contact force can be positive; and these three constraints constitute a complementarity condition that can be denoted by $\mathbf{0} \leq \gamma \perp \phi(\mathbf{q}) \geq \mathbf{0}$.

Recently, Manchester & Kuindersma [9] proposed a variational contact-implicit trajectory optimization that is similar

to [3]. However, in [9], equality constraints in complementarity conditions are relaxed through slack variables to improve the convergence, as in [23], by allowing positive contact forces from distance but they also penalize this term and minimize deviation from strict rigid-body contact. In this work, we use a similar approach and relax (5) through a slack variable $s \geq 0$ that determines the deviation from the strict rigid-body contact:

$$\gamma^T \phi(\mathbf{q}) \leq s. \quad (6)$$

Consequently, (2), (3), and (5) form the complementarity constraints-based contact model that we use in this study.

2) *Smooth Contact Model:* Relaxing the equality constraint in the complementarity constraints provides a smoother contact model; however, using such a model is restrictive since it requires a constrained optimization algorithm. On the other hand, using directly a smooth contact model, such as those in [10–12], would eliminate this limitation. In this study, we use the following exponential formulation for the magnitude of the normal contact force, γ , that is based on the contact model proposed in [12] and analogous to a spring model:

$$\gamma(\mathbf{q}) = k_s e^{(-\alpha_k \phi(\mathbf{q}))}, \quad (7)$$

where k_s is the spring stiffness and α_k determines the curvature of the contact force with respect to the distance, $\phi(\mathbf{q})$. We neglect the damping component in the original spring-damper model for the sake of simplicity. Figure 1 shows the variation of the magnitude of the normal contact force, γ , vs. the distance, $\phi(\mathbf{q})$, with negative distance being penetration to the contact surface.

3) *Variable Smooth Contact Model:* In the smooth contact model, a fixed value for each parameter is selected such that the convergence of gradient-based optimization is satisfactory. In other words, discovery of contacts is facilitated by allowing, albeit very small, contact forces to act from distance at the cost of loss in physical fidelity. As a consequence, there is a trade-off between the physical accuracy and the convergence of optimization. Thus, the parameters need to be tuned very sensitively based on the task. In order to mitigate this problem, we propose a variable soft contact model in which the spring stiffness k_s is a decision variable of optimization, and the curvature parameter is a function of k_s , i.e., $\alpha_k = c/k_s$ where c is a constant.

In Fig. 1, for the first three curves (indicated by red, yellow, and green), $c = 10^3$; and for the remaining curves, $c = 5 \times 10^3$. In this study, we used the greater value for c because the distance - contact force relation converges to a rigid-body contact model as k_s becomes smaller, while it is more similar to a soft contact model for the smaller c . It is also noted that the contact force due to this contact model completely vanishes when $k_s = 0$.

Using small values for k_s is possible when tasks such as locomotion are considered because usually either there are existing contacts or the distances between the contact candidates on the robot and the environment are not very large. Nevertheless, if one considers a manipulation task that

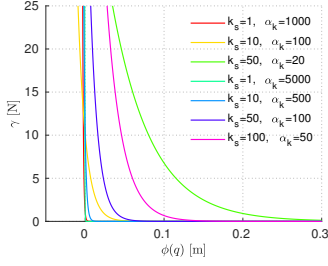


Fig. 1. Variation of the magnitude of the normal contact force with respect to the distance for various stiffness and curvature values.

requires, e.g., pushing an object that is far away from the robot, it is necessary to use a much larger k_s in order for the optimization to be able to discover such motions. However, a large k_s becomes problematic as the distance goes to zero. Thus, the VSCM allows the optimization to handle k_s as necessary.

C. Contact-Implicit Trajectory Optimization

In the contact-implicit trajectory optimization, the main goal is to find contact forces along with control inputs given a high-level definition of the task in terms of a cost function and constraints. The optimal control problem of trajectory optimization (i.e., an infinite-dimensional problem) can be converted into a finite-dimensional problem through transcription methods which can be divided into three categories as single shooting, multiple shooting, and direct transcription [24]. In this study, we transcribe the problem into a single-shooting optimization problem by using evenly separated collocation points for the control inputs, u , and contact model-related parameters.

We consider the task of nonprehensile manipulation of pushing a cubic object on a tabletop by a 7 DOF robotic arm. The corresponding cost function can be written in terms of final costs and integrated costs. In this case, the final costs are based on the normalized distance of the object's center of mass (CoM) from a desired position, \mathbf{p}_o^e , and the change of the object's orientation, θ_o , that is measured by the angle between the initial and final orientation vectors of the x -axis of the object frame; while the integrated costs are based on the end-effector velocity, $\dot{\phi}(\mathbf{q}, \dot{\mathbf{q}})$, and the magnitude of the normal contact force, γ . Moreover, we normalize these cost terms such that the final position error is divided by the initial position error, which yields $\mathbf{p}_{o,normalized}^e$, and the integrated costs are divided by N so that the optimization process is less sensitive to the task and the duration. Then, the final and integrated components of the task-related part of the cost function (c_t^f and c_t^i , respectively) are calculated in terms of the weights w_1, \dots, w_4 , the control sampling period T_c , the time step k , and the number of time steps N by:

$$c_t^f = w_1 \|\mathbf{p}_{o,normalized}^e\|_2^2 + w_2 \theta_o^2, \quad (8)$$

$$c_t^i = \frac{T_c}{N} \sum_{k=1}^N (w_3 \|\dot{\phi}_k(\mathbf{q}_k, \dot{\mathbf{q}}_k)\|_2^2 + w_4 \|\gamma_k\|_2^2). \quad (9)$$

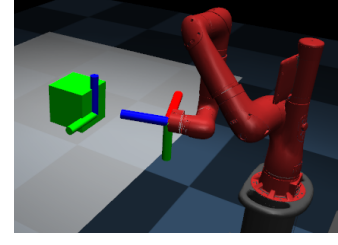


Fig. 2. Simulation environment in MuJoCo and the frames associated with the contact candidates on the robot and the object.

Following optimization problems are solved by the SQP-based solver SNOPT by running forward simulations in MuJoCo to evaluate cost and constraint functions.

1) *Optimization Problem for CCCM*: The optimization problem that includes the relaxed complementarity constraints is defined as:

$$\underset{\mathbf{u}_1, \dots, \mathbf{u}_N, \gamma_1, \dots, \gamma_N, s_1, \dots, s_N}{\text{minimize}} \quad c_t^f + c_t^i + w_5 \sum_{k=1}^N s_k^2 \quad (10a)$$

subject to

$$\phi_k(\mathbf{q}), \gamma_k, s_k \geq 0 \text{ for } k = 1, \dots, N \quad (10b)$$

$$\phi_k^T(\mathbf{q}) \gamma_k \leq s_k \text{ for } k = 1, \dots, N \quad (10c)$$

For this problem, the weights are selected as $w_1 = 10^4$, $w_2 = 10^4$, $w_3 = 2 \times 10^{-1}$, $w_4 = 2 \times 10^{-1}$, and $w_5 = 10^3$.

2) *Optimization Problem for Smooth Contact Models*: The optimization problem takes the following unconstrained form for smooth contact models:

$$\underset{\mathbf{u}_1, \dots, \mathbf{u}_N, (k_{s,1}, \dots, k_{s,N})}{\text{minimize}} \quad c_t^f + c_t^i. \quad (11)$$

The only difference is that the stiffness for each control time step $k_{s,i}$ is a decision variable for the variable SCM. The weights for both problems are same and selected as $w_1 = 10^3$, $w_2 = 10^3$, $w_3 = 2 \times 10^{-1}$, and $w_4 = 2 \times 10^{-2}$.

III. SIMULATION EXPERIMENTS

A. Experimental Setup

The algorithms are tested in simulation for a simple scenario of pushing a cubic object on a tabletop with a Sawyer robot that has a 7 DOF arm. In order to keep the complexity of the task low for the sake of comparison, we consider a simple pushing task in which the initial position of the object's CoM is $x = 1.25$ m, $y = 0$ m, $z = 0.1$ m and the desired position is $x = 1.5$ m, $y = 0$ m, $z = 0.1$ m; i.e., a translational motion along the x -axis. Therefore, we take into account only two contact candidates: one on the object that is on the closest surface of the object to the robot, and one at the center of the end-effector plate of the robot. The simulation environment and the contact frames associated with the contact candidates on the robot and the object are depicted in Fig. 2. Nonetheless, it is noteworthy that the robot can make contact at arbitrary positions on its surface thanks to MuJoCo.

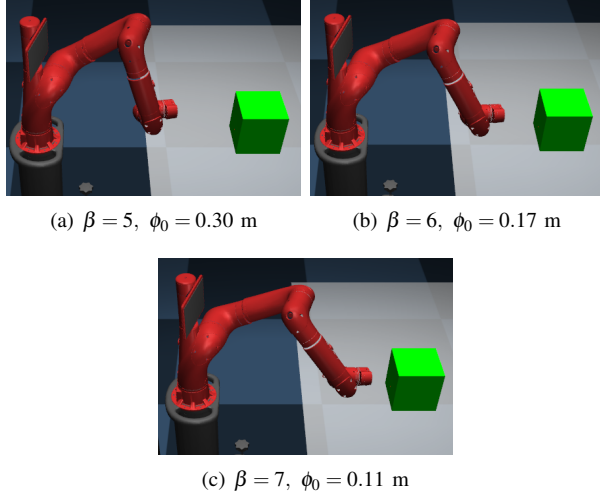


Fig. 3. The initial configurations of the robot for different values of β .

For all simulations, the duration is 1 s, and the control sampling period $T_c = 50$ ms, i.e., $N = 20$. We determine the initial configuration of the arm through the following function of β that also determines the distance between the contact candidates:

$$\mathbf{q}_0 = [-\pi/12, -\pi/\beta, 0, 3\pi/\beta, -\pi/6, -2\pi/\beta, 0]^T$$

We run simulations for three different values of β that are 5, 6, and 7, and the corresponding initial distances between the contact candidates are 0.30 m, 0.17 m, and 0.11 m, respectively. Figure 3 demonstrates the three initial configurations of the arm. It is seen that not only the initial position but also the orientation of the end effector vary depending on β . The purpose of different initial configurations is to change the complexity of the task in a controlled manner by assuming that difficulty in discovering contacts augments as the distance increases.

The stiffness parameter of the SCM is selected as 100 after a careful tuning considering the overall performance, and the corresponding a_k is calculated by $c = 5 \times 10^3/k_s$, as in the VSCM. We use the same value to initialize and upper bound \mathbf{k}_s in the VSCM-based optimization (VSCMO). This value seems reasonable when one looks at the distance range here and the γ vs. $\phi(\mathbf{q})$ curves in Fig. 1.

B. Visual Analysis

In order to see the discrepancies between motions that are optimized by assuming different contact models, we visualize the resulting motions in the following.¹ First, a motion found by the CCCM-based optimization (CCCMO) is shown in Fig. 4. In this motion, the first contact is established at $t=470$ ms, and it is seen that it occurs at the contact candidates on the robot and the object. Then, the contact starts to slide towards the right hand side by causing an undesired rotation of the object along with the desired translation. After the contact is broken, the arm rises because of the impact.

¹Please watch the accompanying video to see the motions for all cases.

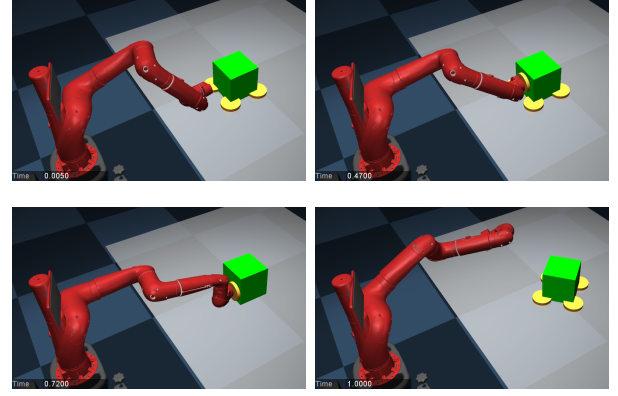


Fig. 4. Snapshots of a resulting motion obtained for the CCCM for $t = 5$, 470, 720, and 1000 ms. Yellow cylinders represent active contacts.

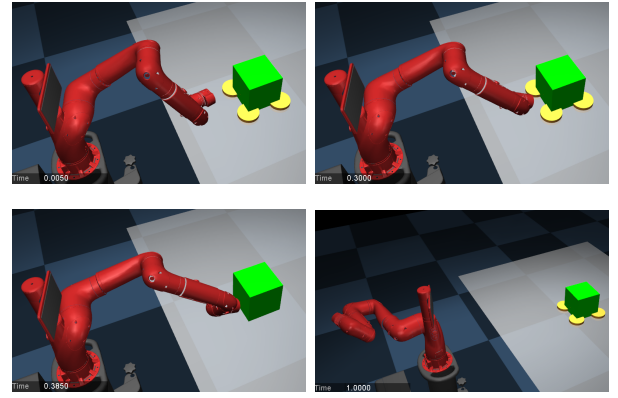


Fig. 5. Snapshots of a resulting motion obtained for the SCM for $t = 5$, 300, 385, and 1000 ms. Yellow cylinders represent active contacts.

Second, Fig. 5 illustrates a resulting motion of the SCM-based optimization (SCMO). The robot approaches the object, and the object is still stationary at $t=300$ ms. However, at $t=385$ ms, the object starts to move due to the force generated by the SCM, even though there is no actual contact between the robot and the object. At the end, the object is successfully manipulated with no visible rotation; yet the arm is repelled significantly due to the large γ values during pushing. The problem of pushing without an actual contact might be alleviated by a very sensitive tuning of k_s ; however, an actual contact still would be very hard to achieve in conjunction with satisfactory motion and convergence. Moreover, repeated sensitive tuning is likely to be necessary even for slight changes in the task, such as the initial configuration of the robot.

Last, a motion obtained from the VSCMO is demonstrated in Fig. 6. Here, the object does not move until there is an active contact at $t=715$ ms. Then, the object is pushed successfully to the desired pose, while the arm is not repelled significantly and stops by making contact with the table. In this case, the arm makes actual contact with the object. This is possible due to the modification of stiffness parameter k_s .

In addition to these, it is clearly seen that the contact at $t=715$ ms occurs at neither of the contact candidates on the

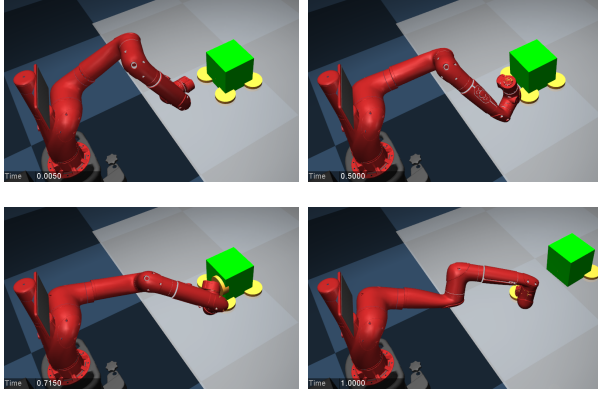


Fig. 6. Snapshots of a resulting motion obtained for the VSCM for $t = 5$, 500, 715, and 1000 ms. Yellow cylinders represent active contacts.

robot nor the object. This is possible due to the fact that the robot can make and break contacts at arbitrary parts of its surface by the virtue of MuJoCo physics engine.

C. Numerical Analysis

After the visual analysis, we investigate the numerical results obtained from the simulations for all the contact models and the initial configurations in the following. First, we focus on the physical fidelity of the resulting motions. In order to measure the physical inaccuracy throughout a simulation, we use a metric that is calculated by integrating the magnitude of the normal contact force acting from distance, i.e., $T_c \sum_{k=1}^N \gamma_k$. Table I shows the values of this metric for all cases. It is seen that the CCCMO provides the best physical fidelity by far for the first two cases. Whereas, the VSCMO has the minimum physical inaccuracy in the last case, i.e., almost zero. Moreover, it provides a much better physical accuracy over the SCMO in all cases.

TABLE I
PHYSICAL INACCURACY METRIC

ϕ_0 [m]	CCCM [N-s]	SCM [N-s]	VSCM [N-s]
0.11	0.1121	2.0400	1.2137
0.17	0.0238	1.4914	1.2676
0.30	0.0373	0.0381	0.0001

Tables II and III summarize the final position and orientation errors for all cases, respectively. It can be seen that in all cases, the VSCMO provides the best performance with respect to the manipulation task, when it is assumed that the differences between the orientation errors for the SCM and VSCM in the first two cases are negligible. Furthermore, it is the only method that can perform the task satisfactorily (i.e., with a position error smaller than 10 cm) for all initial configurations. On the other hand, the SCMO is able to perform the task successfully except for the last case; while the CCCMO can (almost) achieve that only for the initial configuration, and even in that case, the orientation error is quite large.

The computation times for all cases are shown in Table IV. We admit that our implementation is significantly slower

TABLE II
FINAL POSITION ERROR

ϕ_0 [m]	CCCM [m]	SCM [m]	VSCM [m]
0.11	0.1052	0.0285	0.0185
0.17	0.1979	0.0318	0.0291
0.30	0.1924	0.1908	0.0836

TABLE III
FINAL ORIENTATION ERROR

ϕ_0 [m]	CCCM [rad]	SCM [rad]	VSCM [rad]
0.11	0.7067	0.0238	0.0533
0.17	0.4022	0.0586	0.0654
0.30	0.3475	0.4547	0.0415

than the state-of-the-art counterparts such as [11] and, in particular, [12]. However, an optimized implementation of the presented methods is out of scope of this work. Here, we are rather interested in comparing them in terms of the convergence speed. Based on these results, it is not possible to say that there is a clear relationship between the initial distance (or the complexity of the task) and the computation time; i.e., there is a positive correlation for the CCCM, a negative correlation for the SCM, and no correlation for the VSCM. However, it is fair to say that in most cases, the SCMO converges significantly (ca. two-times) faster than the VSCMO – by considering the difference between their computation times for the second case is relatively small. On the other hand, the CCCMO has the slowest convergence speed except for the first case in which its computation time is slightly larger than SCM.

TABLE IV
COMPUTATION TIME

ϕ_0 [m]	CCCM [s]	SCM [s]	VSCM [s]
0.11	43.09	41.07	111.22
0.17	44.52	27.87	16.28
0.30	112.77	23.98	60.49

D. Variation of Stiffness for VSCMO

Finally, the k_s trajectories obtained from the VSCMO are depicted in Fig. 7 for all initial configurations. It is seen that the optimization handles the stiffness k_s as if it is a binary variable; i.e., k_s is either around 100, its initial value and the upper bound, or equal to zero. The collocation points when it is equal to zero correspond to the instants of the simulation when there is an active contact. Hence, in the VSCMO, contacts can be easily discovered from distance as in the SCMO, in addition to the fact that the robot can actually contact the object to move it, as distinct from the case for the SCM with fixed parameters (see Figs. 5 and 6). Moreover, this can be achieved for a wide range of tasks without a sensitive tuning of the contact model parameters.

IV. CONCLUSIONS

In this paper, we analyze the impacts of contact model on the performance of contact-implicit trajectory optimization

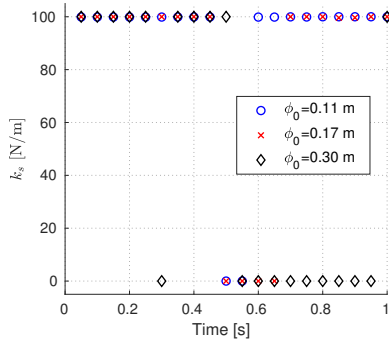


Fig. 7. k_s trajectories found by the VSCM-based optimization for the three values of the initial distance between the contact candidates.

for manipulation. The trajectory planning method in question is a single shooting optimization. Three different contact modeling approaches are investigated: (1) a complementarity constraints-based contact model, (2) a smooth contact model, and our proposed method (3) a variable smooth contact model. We perform simulations by considering the Sawyer robot, which has a 7 DOF arm, that performs a simple manipulation task consisting in pushing a cubic object on a tabletop for different levels of complexity. An analysis of the resulting trajectories yields the following observations. First, all of the methods are capable of discovering a pushing motion given zero initial values for the decision variables. Second, the proposed VSCMO approach is the most reliable since it finds satisfactory motions for all initial configurations. Third, the VSCMO also provides the best performance when the quality of the motions discovered and the physical accuracy are considered; notwithstanding, it has a lower convergence speed than the SCMO which outperforms the CCCMO in all cases. However, the SCMO is very sensitive to the parameters of the SCM, and therefore, it is hard to tune the SCM for a range of tasks. On the other hand, the VSCM allows the optimization to vary the parameters of the contact model as necessary. Consequently, the VSCMO is more robust to changes in the task and, thus, more suitable for contact-implicit trajectory optimization for manipulation.

Nevertheless, the task we investigate here in this paper is limited to one contact candidate on both the robot and the object. We aim to test the proposed method on more complex tasks and behaviours. Furthermore in future work we aim to implement our proposed method experimentally.

REFERENCES

- [1] D. E. Stewart and J. C. Trinkle, "An implicit time-stepping scheme for rigid body dynamics with inelastic collisions and coulomb friction," *International Journal for Numerical Methods in Engineering*, vol. 39, no. 15, pp. 2673–2691, 1996.
- [2] M. Anitescu and F. A. Potra, "Formulating dynamic multi-rigid-body contact problems with friction as solvable linear complementarity problems," *Nonlinear Dynamics*, vol. 14, no. 3, pp. 231–247, 1997.
- [3] M. Posa, C. Cantu, and R. Tedrake, "A direct method for trajectory optimization of rigid bodies through contact," *The International Journal of Robotics Research*, vol. 33, no. 1, pp. 69–81, 2014.
- [4] K. Yunt and C. Glocker, "Trajectory optimization of mechanical hybrid systems using sumt," in *Advanced Motion Control, 2006. 9th IEEE International Workshop on*. IEEE, 2005, pp. 665–671.

- [5] C. Mastalli, I. Havoutis, M. Focchi, D. G. Caldwell, and C. Semini, "Hierarchical planning of dynamic movements without scheduled contact sequences," in *Robotics and Automation (ICRA), 2016 IEEE International Conference on*. IEEE, 2016, pp. 4636–4641.
- [6] Y. Tassa, T. Erez, and E. Todorov, "Synthesis and stabilization of complex behaviors through online trajectory optimization," in *Intelligent Robots and Systems (IROS), 2012 IEEE/RSJ International Conference on*. IEEE, 2012, pp. 4906–4913.
- [7] I. Mordatch, K. Lowrey, and E. Todorov, "Ensemble-cio: Full-body dynamic motion planning that transfers to physical humanoids," in *Intelligent Robots and Systems (IROS), 2015 IEEE/RSJ International Conference on*. IEEE, 2015, pp. 5307–5314.
- [8] M. Neunert, F. Farshidian, and J. Buchli, "Efficient whole-body trajectory optimization using contact constraint relaxation," in *Humanoid Robots (Humanoids), 2016 IEEE-RAS 16th International Conference on*. IEEE, 2016, pp. 43–48.
- [9] Z. Manchester and S. Kuindersma, "Variational contact-implicit trajectory optimization," in *Proceedings of the International Symposium on Robotics Research (ISRR), Puerto Varas, Chile, 2017*.
- [10] T. Marcucci, M. Gabiccini, and A. Artoni, "A two-stage trajectory optimization strategy for articulated bodies with unscheduled contact sequences," *IEEE Robotics and Automation Letters*, vol. 2, no. 1, pp. 104–111, 2017.
- [11] M. Neunert, F. Farshidian, A. W. Winkler, and J. Buchli, "Trajectory optimization through contacts and automatic gait discovery for quadrupeds," *IEEE Robotics and Automation Letters*, vol. 2, no. 3, pp. 1502–1509, 2017.
- [12] M. Neunert, M. Stubler, M. Gifthalder, C. D. Bellicoso, J. Carius, C. Gehring, M. Hutter, and J. Buchli, "Whole-body nonlinear model predictive control through contacts for quadrupeds," *arXiv preprint arXiv:1712.02889*, 2017.
- [13] I. Mordatch, E. Todorov, and Z. Popovic, "Discovery of complex behaviors through contact-invariant optimization," *ACM Transactions on Graphics (TOG)*, vol. 31, no. 4, p. 43, 2012.
- [14] I. Mordatch, Z. Popovic, and E. Todorov, "Contact-invariant optimization for hand manipulation," in *Proceedings of the ACM SIGGRAPH/Eurographics symposium on computer animation*. Eurographics Association, 2012, pp. 137–144.
- [15] S. Jain, Y. Ye, and C. K. Liu, "Optimization-based interactive motion synthesis," *ACM Transactions on Graphics (TOG)*, vol. 28, no. 1, p. 10, 2009.
- [16] D. Zimmermann, S. Coros, Y. Ye, R. W. Sumner, and M. Gross, "Hierarchical planning and control for complex motor tasks," in *Proceedings of the 14th ACM SIGGRAPH/Eurographics Symposium on Computer Animation*. ACM, 2015, pp. 73–81.
- [17] M. Gabiccini, A. Artoni, G. Pannocchia, and J. Gillis, "A computational framework for environment-aware robotic manipulation planning," in *Robotics Research*. Springer, 2018, pp. 363–385.
- [18] E. Todorov, T. Erez, and Y. Tassa, "MuJoCo: A physics engine for model-based control," in *Intelligent Robots and Systems (IROS), 2012 IEEE/RSJ International Conference on*. IEEE, 2012, pp. 5026–5033.
- [19] T. Erez, Y. Tassa, and E. Todorov, "Simulation tools for model-based robotics: Comparison of bullet, havok, mujoco, ode and physx," in *Robotics and Automation (ICRA), 2015 IEEE International Conference on*. IEEE, 2015, pp. 4397–4404.
- [20] P. E. Gill, W. Murray, and M. A. Saunders, "SNOPT: An SQP algorithm for large-scale constrained optimization," *SIAM Rev.*, vol. 47, pp. 99–131, 2005.
- [21] A. W. Winkler, "IFOPT - interface to nonlinear programming solvers IPOPT and SNOPT."
- [22] R. Fletcher, S. Leyffer, D. Ralph, and S. Scholtes, "Local convergence of SQP methods for mathematical programs with equilibrium constraints," *SIAM Journal on Optimization*, vol. 17, no. 1, pp. 259–286, 2006.
- [23] R. Fletcher and S. Leyffer, "Solving mathematical programs with complementarity constraints as nonlinear programs," *Optimization Methods and Software*, vol. 19, no. 1, pp. 15–40, 2004.
- [24] J. T. Betts, "Survey of numerical methods for trajectory optimization," *Journal of guidance, control, and dynamics*, vol. 21, no. 2, pp. 193–207, 1998.